Available online at www.sciencedirect.com
ScienceDirect
Journal of the European Ceramic Society 28 (2008) 3177–3188
www.elsevier.com/locate/jeurceramsoc

Oxidation of titanium carbide–graphite hetero-modulus ceramics with low carbon content
II. Physico-chemical interpretation of the ridge effect

Igor L. Shabalin [a,*], Daniel L. Roach [a], Leonid I. Shabalin [b]

[a] *Institute for Materials Research, The University of Salford, Greater Manchester M5 4WT, UK*
[b] *Russian State Professional and Pedagogical University, Yekaterinburg 620012, Russia*

Available online 24 June 2008

Abstract

Hetero-modulus ceramics (HMC) present the combination of a ceramic matrix with the inclusions of a dispersed phase with considerably lower Young's modulus, resulting in a material with significantly improved properties. An interpretation of the so-called "ridge effect" observed during the isobaric-isothermal oxidation of 93 vol% TiC–7 vol% C (graphite) HMC at temperatures of 400–1000 °C and oxygen pressures of 0.13–65 kPa is given. Established in Part I of this study, the meanings of a ridge temperature and ridge oxygen pressure, which are served as boundaries between prevailing oxidation mechanisms in phenomenological kinetics model, are considered on the basis of X-ray diffraction (XRD) and microscopy analyses. The oxidation mechanisms, essentially different within the studied ranges of temperatures and oxygen pressures are identified according to the developed general model. These results can be used for the preparation of special protective coatings on the surface of refractory carbide–carbon HMC parts applied in severe environments, e.g. chemically active, high-enthalpy gaseous flows.

Keywords: Composites; Chemical properties; Carbides; Carbon; Hetero-modulus ceramics; TiC

1. Introduction

Hetero-modulus ceramic–ceramic composite materials (HMC) present the combination of ceramic matrix having a high-Young's modulus (300–600 GPa) with inclusions of a dispersed phase with significantly lower values (15–20 GPa), such as sp^2-structured graphite and graphite-like hexagonal boron nitride.[1–8] Typical representatives of this sub-class of ceramics are compositions of group 4 transition-metal refractory carbides with excessive carbon,[3,7,8] present in a variety of micro- and nanostructures. In addition to the excellent thermal shock resistance and remarkable machinability inherent to all kinds of HMC, this group of ultra-high-temperature ceramics has another significant advantage: during oxidation at elevated temperatures, the refractory carbides form high-melting scales, which (at least theoretically) could protect the material from further corrosion damage. Carbon–carbon composites (CCC), currently widely used in aerospace engineering as thermal protection for aerodynamically heated surfaces and critical cross-sections of nozzles for rocket engines, demonstrate low gas-corrosion resistance at higher temperatures, so this type of composites needs to be coated with special materials, although this is frequently impractical due to weak adhesion with the substrate.

If the scales formed on HMC possess protective properties and prevent corrosion propagation, the chemical stability of carbide–carbon HMC in active gaseous and melt media will become significantly higher than those for CCC. The advanced physical properties inherent to ceramic matrices, along with high gas-corrosion resistance, provide a good justification for replacement of such carbon composites with HMC. Nevertheless, in spite of the fact that oxide phases individually have good physico-mechanical properties as well as excellent chemical stability in oxidative atmospheres, the oxide scales resulting from the interaction between carbide and oxygen often do not effectively inhibit the oxidation process of the bulk material and provide the corrosion resistant properties that are so desirable. This situation increase the importance of studies devoted to the oxidation processes in the carbide–carbon HMC with different compositions and carbon content. During the comprehensive phenomenological kinetics analysis of the oxidation process for 93 vol% TiC–7 vol% C (graphite) HMC, carried out in Part I

* Corresponding author. Tel.: +44 161 295 3269; fax: +44 161 295 5575.
E-mail address: i.shabalin@salford.ac.uk (I.L. Shabalin).

0955-2219/$ – see front matter © 2008 Elsevier Ltd. All rights reserved.
doi:10.1016/j.jeurceramsoc.2008.04.036

of this work[8] at temperatures of 500–1000 °C and oxygen pressures of 0.13–65 kPa, it was revealed that the behaviour of this material, described using a linear–paralinear model, is unusual, as there was no steady increase of oxidation rate from the lowest temperatures and pressures to the highest ones. However, within the range of studied oxidation temperatures and pressures, there was a clearly defined maximum interaction between solid and gas, which corresponds to critical values of the oxidation parameters. These critical, so-called "ridge" temperatures and pressures mark a change in the prevailing oxidation mechanism; while traversing these features, the values of apparent activation energies Q and orders of reaction m change their signs. This formalism clearly defines regions in parameter space with alternating values (negative and positive) of Q and m, modeling a rather unique phenomenon in solid-state chemistry.

The main aim of Part II of this work is to offer an explanation for this unusual behaviour, revealed while modeling the oxidation kinetics of 93 vol% TiC–7 vol% C (graphite) HMC, by means of an exploration of the physico-chemical transformations and phase transitions associated with this process. There have been few works on the oxidation of HMC containing TiC,[3,9,10] which mainly deal with the comparative evaluation of corrosion resistance for the materials without thorough consideration of the phases generated as reaction products, over the range of temperatures and pressures studied. In spite of the fact that transition-metal carbide phases in HMC possess a specific character[7] and differ from hypostoichiometric MeC_{1-x}, conventionally used in various studies on oxidation, it was impossible to ignore the results obtained from experiments on single-phase samples of TiC, reported by several authors, including recent complex research on oxidation of refractory carbides published by Shimada et al.[11–15] and Gozzi et al.[16,17] The most relevant data available in the literature on physico-chemical analysis of the oxidised materials based on TiC are collected in Table 1. A closer examination of these data shows that, even for the oxidation of individual carbide phases, there are few recognizable details of the underlying reaction mechanism: the formation of non-stoichiometric phases of oxycarbide TiC_xO_y and the presence of two modifications to the TiO_2 structure in the oxidation products with the anatase phase being observed at lower temperatures than the rutile. At the same time many details of the TiC oxidation process, which are connected in particular with carbide–oxide transformation and phase transitions in formed TiO_2, have not been well understood. The results of a number of published works not only differ markedly from those obtained in similar studies, but also have contradictory conclusions: for example, Voitovich and Pugach[24] attribute mutually exclusive effects to deposited carbon, proposing it promotes sintering of oxide scale and stabilises anatase simultaneously.

As a result, being a corollary to the main aim of study, an effort has been made to address the key issues associated with the oxidation of individual carbide phases such as a scheme for the carbide to oxide transformation, the temperature and oxygen pressure ranges of these transformations, also associated with the anatase to rutile transition, and the influence of carbon on these physico-chemical processes. Although the latter problem in the case of the oxidation of HMC is more complicated as an oxidised material can contain two different sources of carbon: "primary" carbon, this being the inclusions of graphite initially introduced as an ingredient of the composite, and "secondary" carbon, which is obtained as a reaction product, during the unique transformation of the oxidised carbide phase.

2. Experimental

The comprehensive details of the physico-chemical characteristics for the studied 93 vol% TiC–7 vol% C HMC (chemical and phase analysis, physical parameters for the components) as well as the full description of employed manufacturing method with a microphotograph of its structure were provided in the previous papers presented to this journal.[7,8] The details of the preparation of HMC samples, exposed to oxygen under different environmental conditions, are described in Part I of this study,[8] including the cutting-off scheme for the hot-pressed ceramic composite blank.

The samples, oxidised at temperatures of 500–1000 °C and oxygen pressures of 0.13–65 kPa, were investigated by the means of X-ray diffraction (XRD), optical and scanning electron microscopy (SEM) analyses as well as microanalysis by electron probe (EMPA) and energy-dispersive X-ray spectroscopy (EDX). The compositions of the sample scales were identified by XRD phase analysis, and the lattice parameters of these phases were measured by means of XRD structural analysis employing a diffractometer DRON-3.0 unit (Bourevestnik, Russia) with filtered Cu K_α radiation. Different cross-sections and surfaces of scale microstructures were investigated by different methods of optical microscopy in an Epitype-2 (Carl Zeiss Jena, Germany) using micro-photo equipment MFN-12 (LOMO, Russia), by SEM and EDX in a Philips XL30 with an embedded EDAX quantitative energy-dispersive spectrometer DX-4i. SEM images were obtained at accelerating voltage $U = 12$–25 kV, employing both secondary electron and back-scattered electron detectors. EMPA was carried out in a MS-46 analyser (Camebax, France).

3. Results and discussion

3.1. Physico-chemical transformations

The evolution of weight gain for the TiC–C HMC samples during the oxidation process, analysed in details in Part I of this work,[8] was accompanied with a change of the chemical composition of the surface layers of the samples. The XRD patterns taken from the surface of the samples, oxidised at lower and higher temperatures, respectively, are shown in Figs. 1 and 2.

No XRD peaks corresponding to the newly formed phases were found on the surface of the oxidised sample for values of weight gain per unit of surface area, $w < 8\ \mathrm{mg\,cm^{-2}}$ (Fig. 1b). However, for all samples oxidised under different conditions, the lattice parameter of the carbide phase changed slightly; for example, at the temperature of 500 °C and oxygen pressure of 1.3 kPa, the lattice parameter reduced from the initial 0.4326 ± 0.0001 to 0.429 ± 0.002 nm. This decrease of lattice

Table 1
Phase analysis of oxidation products for different materials based on titanium carbide

Material (composition, manufacturing method)	Gaseous reagent	Gas pressure (kPa)	Temperature (°C)	Phase analysis of oxidation products[a]	Carbon content in scale (at%)	Reference
TiC_{1-x}, $x = 0.97$; 0.63, sintered (97%)[b]	O_2	~100	900–1000	TiO_2^{ru} (2-layered)	0.33	18
TiC_{1-x}, polycrystalline pyrolytic	O_2	~100	600–1000	TiO_2^{ru} (3-layered)	1.1	19
TiC_{1-x}, sintered (97%)[b]	O_2 (flow)	~100	300–450 450–700 700–1000	TiO_2^{an} Not identified TiO_2^{ru}	– – –	20
TiC_{1-x}, powdered	O_2	0.8–86	600–850	TiO_2^{ru}	–	21
TiC_{1-x}, single crystal	O_2	86	900–1000	TiO_2^{ru} (2-layered)	–	
TiC_{1-x}, $x = 1.00$, single crystal	O_2, O_2/Ar	0.01 1.3–40 96	1015 815–1215 690–1015	TiO_2^{ru} TiO_2^{ru} TiO_2^{ru}	– – –	22
TiC_{1-x}, $x = 0.94$[c], hot-pressed (97%)[b]	O_2	98 98 0.01–30	700–800 900–1200 1100	(TiC_xO_y, Ti_2O_3), **TiO_2^{ru}** (TiC_xO_y), TiO_{2-x}^{ru}, **TiO_2^{ru}** (TiC_xO_y), TiO, (Ti_2O_3, Ti_3O_5), TiO_{2-x}^{ru}, **TiO_2^{ru}**	– – –	23
TiC_{1-x}, $x = 0.97$, powdered	O_2/Ar	3.9–16[d]	400	(Ti_xO, TiO, Ti_2O_3, Ti_3O_5, Ti_4O_7), **TiO_2^{an}**, TiO_2^{ru}	–	11
TiC_{1-x}, $x = 0.97$, powdered	O_2/Ar	2–60[d]	400–600 600–700 700–800 800–900	(TiC_xO_y), TiO_2^{an} (TiC_xO_y), TiO_2^{an}, TiO_2^{ru} (TiC_xO_y), TiO_2^{an}, **TiO_2^{ru}** (TiC_xO_y), TiO_2^{ru}	– – – –	12
TiC_{1-x}, $x = 0.96$, single crystal	O_2/Ar	0.08[d]	1300–1500	Ti_3O_5, **TiO_2^{ru}**	7–23/4–5/2–5[e]	13
TiC_{1-x}, $x = 0.97$, powdered	O_2/Ar O_2/H_2O/Ar O_2/H_2O/Ar	5/95 5/5–10/90 5/5–10/90	320–400 320–350 400	TiO_2^{an} TiO_2^{an} TiO_2^{an}, TiO_2^{ru}	– – –	14
TiC_{1-x}, HIPed (>98%)[b]	O_2/Ar O_2/H_2O/Ar	5/95 5/5/90	900–1200 900–1200	(TiC_xO_y), TiO_2^{ru} (TiC_xO_y), TiO_2^{ru}	– –	15
TiC_{1-x}, $x = 0.97$[c], sintered	O_2/Ar	0.013[d]	865	TiO_2^{ru}	–	16
TiC_{1-x}, $x = 0.93$, single crystal	O_2/Ar	0.024[d]	835	(TiC_xO_y), TiO_2^{ru}	–	17
TiC_{1-x}, $x \sim 1.0$, hot-pressed and annealed (>98%)[b]	Air	~100	700 800–900 1000 1100 1200	TiO, Ti_2O_3 TiO, Ti_2O_3, TiO_2^{an}, TiO_2^{ru} Ti, TiO, Ti_2O_3, TiO_{2-x}^{ru}, TiN Ti, TiO, Ti_3O_5, TiO_2^{an}, TiO_2^{ru}, TiN Ti, (TiO), TiO_2^{ru}	– – – – –	24
TiC_{1-x}, $x = 0.96$; 0.94, hot-pressed (96–97%)[b]	Air	~100	800–1200	(TiC_xO_y), TiO_2^{ru}	–	25
TiC–C, hot-pressed (97%)[b]	O_2	1.3–13	500–600 700–800 900–1000	(TiC_xO_y), TiO_2^{an} (TiC_xO_y), TiO_2^{an}, TiO_2^{ru} (TiC_xO_y), TiO_2^{ru}	–	3
(Ti, Cr)C–C, fused	Air	~100	1000, 1550	(TiC_xO_y), TiO_2^{ru}, ω-TiO_2·Cr_2O_3	–	9

[a] The prevailing phases are printed in bold type, trace amounts of phases are shown in parenthesis.
[b] Relative density in percents with theoretical.
[c] Calculated from the experimental data.
[d] Partial pressure of O_2.
[e] Contents in inner/intermediate/outer layers, respectively.

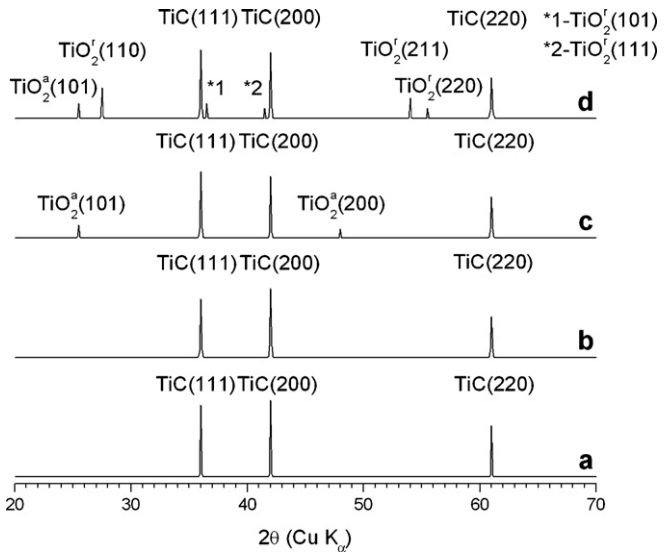

Fig. 1. XRD patterns of the 93 vol% TiC–7 vol% C HMC samples oxidised at lower temperatures: (a) initial material; (b) $T = 500\,^{\circ}C$, $p_{O_2} = 1.3$ kPa; (c) $T = 600\,^{\circ}C$, $p_{O_2} = 1.3$ kPa; (d) $T = 700\,^{\circ}C$, $p_{O_2} = 1.3$ kPa (indices relate to different polymorphic crystalline modifications of titanium dioxide: *a*, anatase; *r*, rutile).

parameter was accompanied by a significant enlargement of the half-widths for all XRD peaks of the carbide phase. The standard deviation for different samples increased to approximately 10–20 times for the 95% confidence interval. However, it proved to be impossible to find any correlations between this change in lattice parameter and values of the oxidation parameters (temperature and oxygen pressure), as the decrease of lattice parameter was approximately equal for all oxidised samples of the XRD patterns obtained.

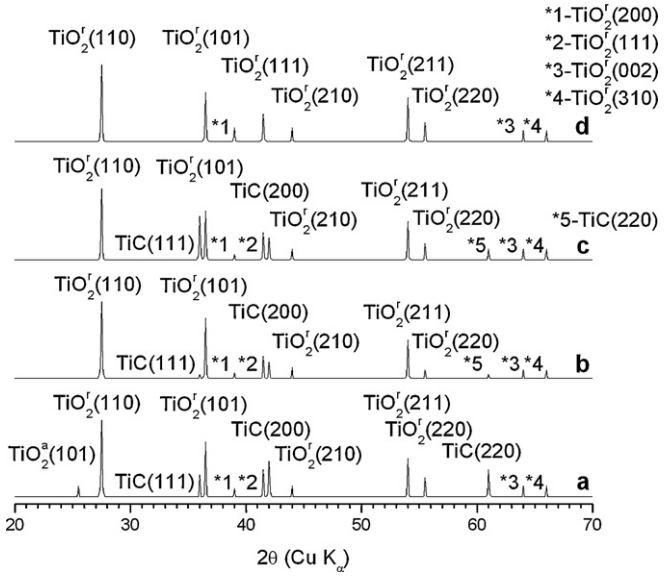

Fig. 2. XRD patterns of the 93 vol% TiC–7 vol% C HMC samples oxidised at higher temperatures: (a) $T = 800\,^{\circ}C$, $p_{O_2} = 1.3$ kPa; (b) $T = 900\,^{\circ}C$, $p_{O_2} = 1.3$ kPa; (c) $T = 1000\,^{\circ}C$, $p_{O_2} = 1.3$ kPa; (d) $T = 1000\,^{\circ}C$, $p_{O_2} = 1.3$ kPa (indices relate to different polymorphic crystalline modifications of titanium dioxide: *a*, anatase; *r*, rutile).

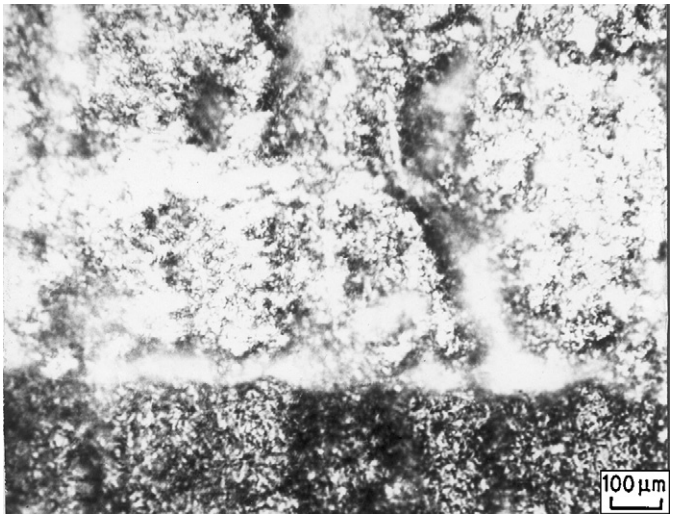

Fig. 3. Microstructures of oxide scale and oxide–composite interface (polarized light) for the 93 vol% TiC–7 vol% C HMC sample oxidised at temperature $T = 700\,^{\circ}C$ and oxygen pressure $p_{O_2} = 1.3$ kPa for 2 h.

The first oxide phase appears at 600 °C and 1.3 kPa (Fig. 1c) and it is represented on the pattern by small broad peaks of TiO_2 (anatase). At 700 °C, the oxide scale consists just of two crystalline structures of TiO_2—anatase and rutile (Fig. 1d). The latter phase becomes predominant at 800 °C and 1.3 kPa when, compared with the carbide and anatase (Fig. 2a), and at $T \geq 900\,^{\circ}C$ and $p_{O_2} \geq 13$ kPa (Fig. 2b), the rutile phase completely replaces the anatase in scale. Even at 1000 °C and 1.3 kPa, the XRD peaks of the carbide are still observed (Fig. 2c). They disappeared only at the highest values of temperature and oxygen pressure used here (Fig. 2d).

Due to the unusual structure of the scales, there are serious difficulties in the preparation of the plane cross-sections of highly oxidised TiC–C HMC samples. Unfortunately, the images from the fractured surfaces for the samples were not sufficiently informative. As a result of these factors, it was not possible to conduct a thorough investigation of the oxide scales, as it appears quantitative measurements of scale properties require an improvement in the preparatory techniques applied in this experiment. The obvious feature of interest for the studied samples is the complicated hierarchy of inhomogenuity inherent to the scales formed on the HMC. It seems likely that the common layered structure of oxide scale, typically observed during the oxidation process of metals and their compounds, breaks down in the case of the HMC samples (Fig. 3), probably, because of the wide development of short-circuit diffusion processes in this type of material.[7] The preparation of objective cross-sections for EMPA also encountered similar difficulties, so the results provided only one finding. This was connected with oxidation at the highest temperatures (as in the samples treated at 900–1000 °C) where depletion of titanium in the inner part of the oxide scale was found, probably due to diffusion of titanium towards the solid–gas interface as was previously revealed for oxidised TiC_{1-x} by Reichle and Nickl.[22]

However, at earlier stages of oxidation, the results obtained by SEM and EDX were more successful, as it was only necessary

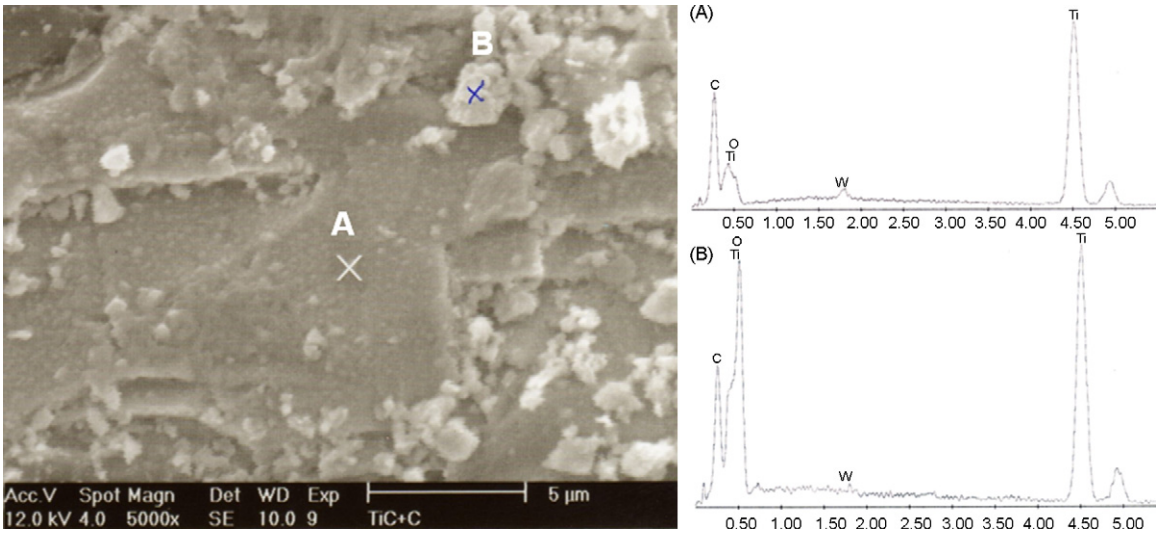

Fig. 4. The SEM micrograph (5000×) and EDX patterns (A and B) for Ti, C, O and W (*X*, energy in keV; *Y*, intensity in a.u.) obtained from the surface of 93 vol% TiC–7 vol% C HMC oxidised at temperature $T = 600\,^{\circ}\mathrm{C}$ and oxygen pressure $p_{O_2} = 1.3\,\mathrm{kPa}$.

to investigate the surface layers of the sample. Employing simultaneous analysis of the structure image and chemical content for the oxidised surface of TiC–C HMC (Fig. 4), it became possible to determine the atomic ratio of $O/Ti = 0.28 \pm 0.05$, which characterises the material and corresponds to the incubation of the oxide on the solid–gas interface.

3.2. Oxidation mechanisms

3.2.1. General remarks

The general scheme of the oxidation process for the TiC–C HMC, presented in Fig. 5, includes several stages, some of which should be considered as concurrent. The experimental data obtained in this study (see also Part I of this work[8]) suggest that this process is very sensitive to both temperature and oxygen pressure and that the oxidation mechanism changes significantly with transfer from lower to higher values of oxidation parameters. The oxidation process itself can be divided into two sub-processes characterised by the different physico-chemical transformations in the HMC:

- the formation of titanium oxide due to oxidation of the carbide phase:

$$\mathrm{TiC}_{1-x} + \mathrm{O}_2 \rightarrow \mathrm{TiC}_{1-x-y}\mathrm{O}_y + \mathrm{C(CO,\ CO_2)} + \mathrm{O}_2 \rightarrow \mathrm{TiO}_z + \mathrm{C(CO,\ CO_2)} \quad (1)$$

and

- the oxidation of carbon with formation of carbon oxides:

$$\mathrm{C} + \mathrm{O}_2 \rightarrow \mathrm{CO,\ CO_2} \quad (2)$$

Here, it should be noted that reaction (2) describes the burn-off for both the graphite phase and "secondary" carbon formed by reaction (1). Although the relationships between these sub-processes may be complex and dependent on oxidation conditions, it appears that the pressure of the same gaseous products determine the reaction equilibrium for both sub-processes, in which carbon itself represents not only a reagent for reaction (2), but also a product of reaction (1).

The dependencies of reaction rates $\mathrm{d}(\Delta m_i)/\mathrm{d}t$ on weight gain w during the oxidation process of the material follow a

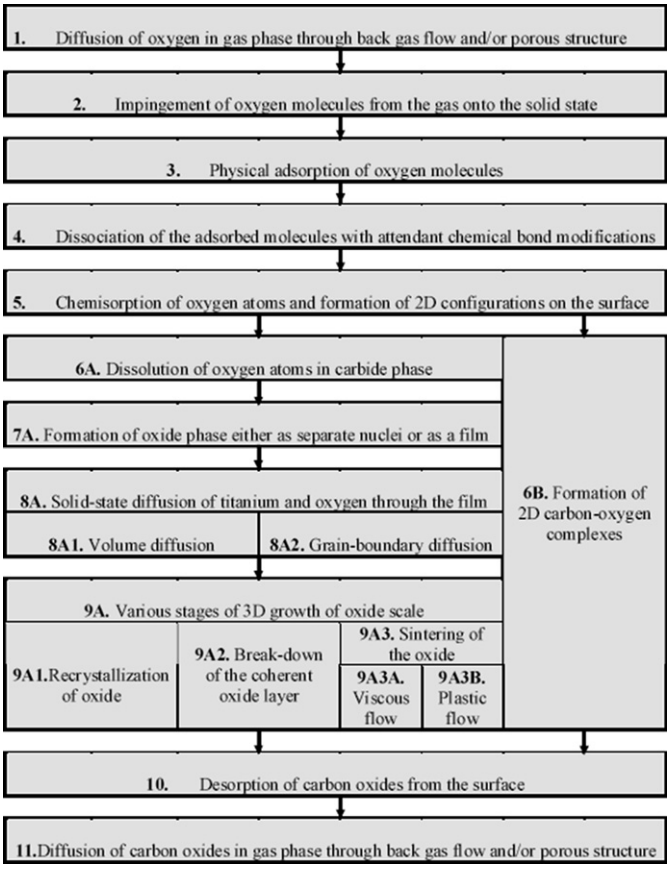

Fig. 5. The general scheme of process stages for the oxidation of TiC–C HMC.

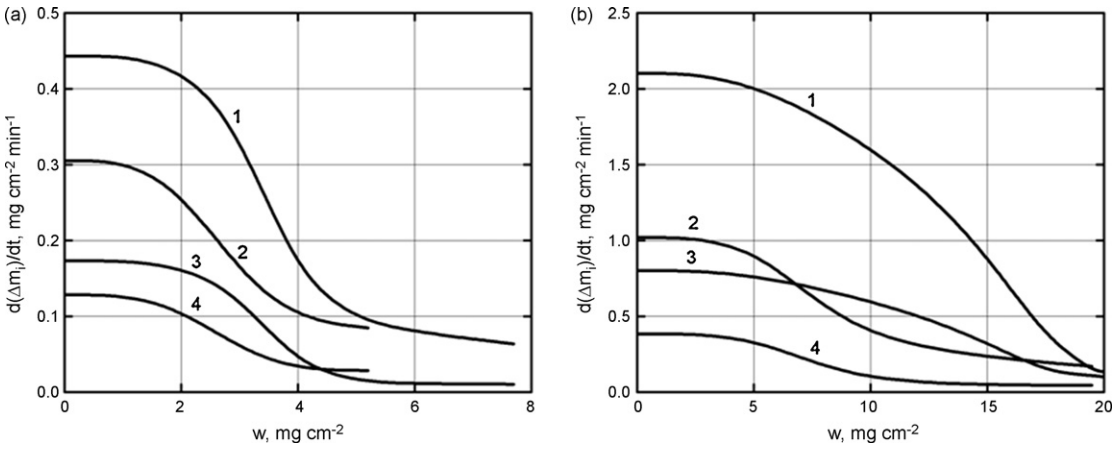

Fig. 6. Plots of $d(\Delta m_i)/dt$ vs. w for oxygen consumption (1 and 2) and carbon burn-off (3 and 4) kinetics during the oxidation of 93 vol% TiC–7 vol% C HMC at different temperatures: (a) $T = 500\,^{\circ}C$; (b) $T = 700\,^{\circ}C$ and oxygen pressures: (2 and 4) $p_{O_2} = 1.3$ kPa; (1 and 3) $p_{O_2} = 1.3$ kPa.

linear–paralinear model[8] for oxygen consumption as well as for carbon burn-off kinetics. As illustrated in Fig. 6, the oxidation of the HMC begins with a period of constant reaction rates (linear stage) followed by a parabolic stage where these reaction rates diminish dramatically. The final linear stage of the process is defined by a return to a constant oxidation rate. This suggests different oxidation mechanisms at work, which evolve over time with transfer of the oxidation process from one stage of the phenomenological kinetics model[8] to another. Independent of this are some ranges of oxidation parameters (temperature and oxygen pressure) over which one definite stage or the transition regime between two adjacent stages of the process (see Fig. 5) begin to dominate over a mechanism as a whole. This, in turn, delivers key information upon which the general model of the oxidation process of the material, based on the kinetics analysis as well as microstructure investigations, can be built.

3.2.2. *Lower temperatures/lower oxygen pressures*

At the lower values of oxidation parameters, 500–700 °C and 0.65–13 kPa, it was found in Part I of this work[8] that the initial linear stage in oxidation kinetics of 93 vol% TiC–7 vol% C (graphite) is characterised by $Q = 45$–70 kJ mol^{-1} with m subse-

Table 2
Relationship between lattice parameter a, nm and stoichiometric coefficients x and y of titanium oxycarbide TiC_xO_y, according to literature data,[17,23,27–31] compared with a for the initial composition TiC–C HMC

x+y / y	0.5-0.6	0.6-0.7	0.7-0.8	0.8-0.9	0.9-1.0	1.0-1.1	1.1-1.2
1.1-1.0						0.4183-0.4220	
1.0-0.9							0.4233
0.9-0.8						0.4232	
0.8-0.7						0.4257-0.4245	0.4274
0.7-0.6			0.4223				
0.6-0.5			0.4247			0.4287--0.4293	
0.5-0.4				0.4286		0.4299--0.4304	
0.4-0.3			0.4282			0.4306--0.4312	
0.3-0.2		0.4280	0.4285--0.4297		0.4310--0.4316	0.4317--0.4319	
0.2-0.1		0.4286--0.4292	0.4306--0.4309		0.4313--0.4323	0.4322	
0.1-0.0	0.4299	0.4314	0.4307--0.4328	0.4331	0.4322--0.4328	**0.4326± ±0.0001**[b]	

[a]The proposed range of existence for TiC_xO_y with $a = 0.429 \pm 0.002$ nm is shaded grey. [b]The lattice parameter of initial carbide phase in the studied HMC. [c]The range for $TiC_{0.90\pm0.15}O_{0.28\pm0.08}$ coexisted with oxide at the earliest stage of oxidation is marked out in bold.

quently increasing from 1/6 at 500 °C to 1/5 at 600 °C and then up to 1/2 at 700 °C. On the basis of information derived from the XRD, SEM and EPMA analyses, it appears reasonable to connect this stage with the dissolution of oxygen in the carbide and formation of the oxycarbide phase $TiC_{1-x-y}O_y$, as described by Eq. (1) for the first reaction. At temperatures of about 500 °C and oxygen pressures of 3.9–16 kPa, Shimada and Kozeki[11] reported a very similar value of Q for the oxidation of TiC_{1-x} powders, but for parabolic kinetics with $m = 0.2–0.6$. They proposed that the diffusion of oxygen through the oxycarbide phase should be responsible for such low value for Q. However, according to Schuhmacher and Eveno,[26] the activation energy of oxygen diffusion in $TiC_{0.97}$ is close to that of carbon, with a value of $383 \pm 8\,kJ\,mol^{-1}$ at 1500–2100 °C; certainly, the value of Q is only slightly lower for the lower temperature range. From this we can conclude that it is more likely that the decomposition of the oxycarbide phases[27–29]oversaturated by oxygen, followed by the formation of oxide nuclei according to reaction:

$$TiC_{1-x-y}O_y \rightarrow TiC_{1-x-y-a}O_z + aC(CO) \rightarrow TiO_{2-b}C_b + dC(CO) \rightarrow TiO_{2-u} + C(CO) \quad (3)$$

acts as the governing stage for the oxidation of carbide or carbide–carbon materials in this case. It was clear that the deviations of lattice parameter for the carbide phase were approximately the same for samples oxidised under different conditions. Hence, according to data available in literature (Table 2), the lattice parameter of 0.429 ± 0.002 nm experimentally obtained in this study corresponds to the oxycarbide, for which the composition is in the range of $TiC_{0.3–0.8}O_{0.1–0.8}$. However, SEM, EDX and EMPA measurements allowed the determination of the composition of oxycarbide (coexisting with rare particles of oxide on the surface of material) as following $TiC_{0.90\pm0.15}O_{0.28\pm0.08}$. Shimada[12] observed similar oxidation behaviour for the individual TiC_{1-x} phase, attributing their findings to a structure with lattice parameter of 0.4327 ± 0.0001 nm and composition of $TiC_{>0.5}O_{<0.5}$.

The subsequent transition to the parabolic kinetic stage leads to a value of activation energy, $Q = 75–105\,kJ\,mol^{-1}$ and exponent m, which increases with temperature increase as observed previously. The variations of m in the interval from 1/6 to 1/2 reflect the solid-state diffusion character of the process and connect with the concentration of oxygen vacancies, as it is in good agreement with data on defect structure of non-stoichiometric p-conductive titanium oxide.[32,33] During this stage, it would appear that the oxidation process transits to the solid-state diffusion regime and the most probable rate-determining stage in this range of temperatures and pressures is oxygen diffusion through the anatase $TiO_{2-b}C_b$ scale (see Fig. 1c). The formation of carbon-doped anatase phase $TiO_{2-b}C_b$ with $b = 0.02/0.05$ as an initial product of TiC_{1-x} oxidation, was confirmed quite recently by Irie et al.[34] as well as Shen et al.[35] at lower temperatures in oxygen and air. There is available data in the literature on the activation energy for the parabolic oxidation of single crystals and polycrystalline TiC_{1-x} by oxygen[21,22] with values close to $200\,kJ\,mol^{-1}$; e.g. Voitovich and Lavrenko[25] determined the value of activation energy, in the interval from 184 to $217.5\,kJ\,mol^{-1}$, to be dependent on the purity of the carbide phase. All of these values are in good agreement with the activation energy of oxidation for titanium metal at the same temperatures, connected with the process of oxygen lattice diffusion.[36] Nevertheless, in the earlier works it was suggested that, at low temperatures and oxygen pressures (500 °C, 13 Pa), a high percentage of the oxide area consists of paths of low diffusion resistance and hence grain boundary diffusion plays an overwhelming role in the oxidation of titanium metal[37] compared to the negligible role played by lattice diffusion. Additionally, relatively low values of oxidation activation energy for the carbide–graphite compositions obtained in this work are clearly connected with the structure of HMC, characterised by a widely developed grain boundary network.[3,7] The short-circuit diffusion along grain boundaries and dislocations in similar materials plays a more important role than it would with single phase refractory carbides in general.[7] However, the activation energy for grain boundary diffusion is smaller than that for lattice diffusion and the value for the former accounts for about a half of the latter in metal oxidation processes,[36] although Rothschild et al.[38] determined this ratio for chemical diffusion in non-stoichiometric TiO_2 films at lower temperatures as 3/4 and the value of Q for grain boundary diffusion of about $50\,kJ\,mol^{-1}$. Yet the dispersion of graphite inclusions in the HMC, forming the structure of the material, is not the only factor contributing to this dominant role for short-circuit diffusion. Other contributing factors, such as the lower temperatures of oxidation ($T \leq 0.5$ of the melting point of TiO_2) and the fine dispersal of residual carbon throughout the oxide scale, also contribute significantly to a predominantly solid-state transport mechanism along low-resistance diffusion paths.

The residual carbon dispersed throughout the scale is a result of non-stoichiometric oxidation of the carbide and the composite material in general, as the fractions of Ti and C oxidised during the gas exposure differ significantly. The total (integral) ratio of

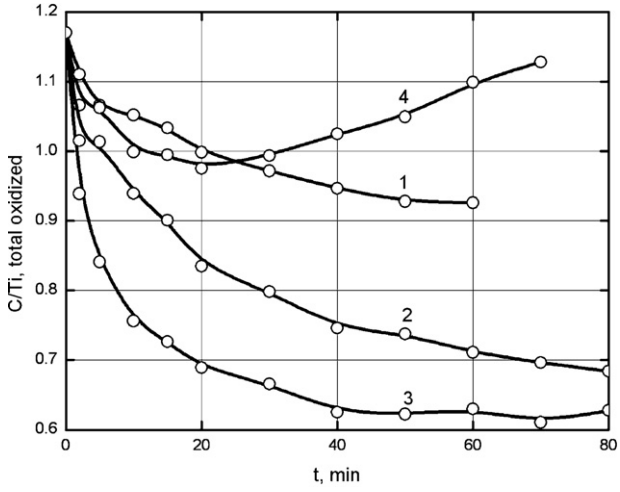

Fig. 7. Evolution of the current value of C/Ti total (integral) oxidised ratio during the oxidation process for 93 vol% TiC–7 vol% C HMC at different temperatures: (1 and 2) $T = 500$ °C; (3 and 4) $T = 700$ °C and oxygen pressures: (1 and 3) $p_{O_2} = 1.3$ kPa; (2 and 4) $p_{O_2} = 1.3$ kPa (calculated by taking into account the formation of TiO_2, CO and CO_2 only).

C/Ti involved in the oxidation process (Fig. 7) was calculated by only taking into account the formation of such oxides as TiO_2, CO and CO_2, as the small contribution of the formation of oxycarbide to the overall process could be safely neglected and no other products were identified in the oxidised samples. However, the analysis showed that, at lower temperatures/lower oxygen pressures, the process of titanium oxide formation generally dominates over the oxygen–carbon interaction. An illustration of this is provided by comparison of the number of titanium atoms entering into reactions with oxygen at 700 °C and 1.3 kPa over an hour with those of carbon; the former is about two times more than the latter, showing a clear dominance of the metal oxide scale producing mechanism. Therefore it is understandable that the grain growth of oxide scale is retarded, not only by initial graphite inclusions, but also by the presence of secondary carbon formed because of the non-stoichiometric oxidation of the combined carbon in the carbide phase.

In general, the shift of the reaction mechanism to short-circuit diffusion is mainly due to the character of carbon oxidation, which lags behind the oxidation of metal Ti (formation of oxide scale). The removal of carbon oxides forms the specific micro- and nanoporous structure of the scales. In keeping with the laminar-nature of most oxide scales, the microstructure is also characterised by some "lateral elements" (see Fig. 3). Initially, these are easy diffusion paths for oxygen, afterwards transformed into the grain boundaries, which are formed by precipitated carbon like those observed by Voitovich and Lavrenko[25] in the oxidised $TiC_{0.96}$. Unfortunately, SEM images are not informative in this case, as it is necessary to develop special quantitative methods of scale characterisation, but it seems obviously that the final period of the oxidation is connected with the initiation of micro- and nanochannels, which are formed by gases escaping the bulk sample.

The transfer of the rate-determining stage of the process from solid-state diffusion to predominantly gas diffusion in the final stage is also evidence of the priority of short-circuit diffusion during the propagation of the oxidation process. At lower temperatures/lower pressures, this stage is described by linear kinetics with $Q = 30$–$40\,\mathrm{kJ\,mol^{-1}}$. The exponent m, growing from 0 at 500 °C to 1/5–1/10 at 600 °C and then up to 1/3 at 700 °C, also supports the suggestion concerning the transition of the prevalent mechanism to gas processes. With reference to these observations, and on the basis of microstructure studies, the most likely rate-determining stage in this case is the transition regime of carbon gasification between the chemical reaction (carbon oxidation) and gas diffusion stages. This conclusion seems credible, as the obtained value for Q is very close to those for the processes controlled by the gas diffusion stage of carbonaceous materials oxidation,[39–41] while m is of the same order as those for the processes dominated by the chemical reaction stage of the carbon oxidation.[42,43]

3.2.3. Lower temperatures/higher oxygen pressures

The increase of oxygen pressure at 500–700 °C up to 13–65 kPa results in the initial linear stage in oxidation kinetics with $Q = 60$–$75\,\mathrm{kJ\,mol^{-1}}$ and negative values of

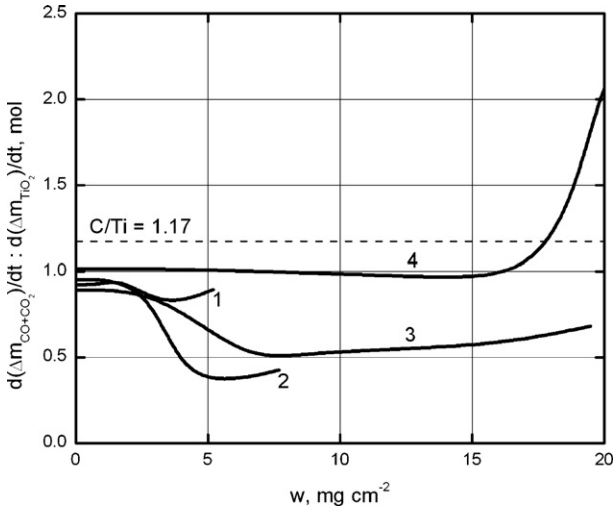

Fig. 8. Plots of $d(\Delta m_{CO+CO_2})/dt : d(\Delta m_{TiO_2})/dt$, in mol vs. w for the oxidation process of 93 vol% TiC–7 vol% C HMC at different temperatures: (1 and 2) $T = 500$ °C; (3 and 4) $T = 700$ °C and oxygen pressures: (1 and 3) $p_{O_2} = 1.3$ kPa; (2 and 4) $p_{O_2} = 1.3$ kPa.

$m = -((1/2)–(1/3))$, so it is suggested that controlling stage of the process shifts from the solid-state diffusion to the transition regime between solid-state and gas diffusion processes. This regime is realised due to the development of sintering and grain growth processes in the scale. The rate of oxidation, being limited by the gas diffusion process, correlates with the characteristics of porosity of the oxide scales because of the influence of these characteristics on gas diffusion (Knudsen flow, surface diffusion, adsorption–desorption processes) through the scale.[44] At the same time, these characteristics are dependent directly on values of the parameters for solid-state diffusion, by which such processes as sintering and grain growth are governed. Although to date there have been no attempts to evaluate quantitatively the relationship between permeability of scale and its recrystallisation temperature, a similar situation with the influence of scale sintering on the reactivity of materials seems to be typical for the oxidation of both individual transition-metal carbides and carbide compositions and very important for analysis of the process.[3,45,46] A key point in the oxidation of the carbides and compositions based on the metal–carbon systems is the contribution of the gas diffusion processes, necessary for the removal of products of carbon gasification, to the overall process of material oxidation as, at moderate temperatures, the solid-state diffusion of residual carbon is significantly retarded. This is the principal difference between the oxidation processes of metal carbides compared with those of pure metals. The difficulties associated with the removal of carbon oxides can noticeably influence the rate of oxidation of carbides in general and appear to be especially important for carbide–carbon HMC oxidation.

The transition in the kinetics model to the parabolic stage at lower temperatures/higher oxygen pressures is characterised by a slight increase of Q to 75–100 kJ mol^{-1}; while m varies widely, it remains negative and increases in absolute value from 1/10 at 500 °C to 1/2 at 600 °C and then up to 1 at 700 °C. The oxidation mechanism does not change and remains in the same transition

regime as in the previous stage, but with a greater contribution from the gas diffusion mechanism, which dominates completely during the subsequent final linear stage. As shown in Fig. 8, this stage differs from those previously by an accelerating carbon burn-off; this effect is clearly evident in plots of C/Ti oxidation rates ratio versus w. The plots, shown in Figs. 7 and 8, also help explain the ridge effect of oxygen pressure at 13 kPa, discussed in details in Part I of this work.[8] During the linear–paralinear oxidation cycle, this pressure appears to be sufficient to enable the oxidised carbon and titanium to reach the C/Ti ratio of the initial materials before oxidation; that is, the ratio C/Ti = 1.17 for the 93 vol% TiC–7 vol% C (graphite) composition studied in this work. At the ridge oxygen pressure, the process of carbon oxidation is "catching up" with the oxidation of titanium metal. Over the studied temperatures and oxygen pressure range from 13 up to 65 kPa, the final linear kinetics stage is characterised by the same values of $Q = 5$–$10\,\mathrm{kJ\,mol^{-1}}$ and slightly variation of $m = 1/2$–$1/3$; sufficient grounds to identify this stage as being regulated by the interdiffusion of oxygen and carbon oxides gas flows through the micro- and nanoporous titanium oxide scales.

3.2.4. Higher temperatures/lower oxygen pressures

The oxidation behaviour of the material at the lowest level of oxygen pressure studied in this work convincingly demonstrated the large influence that sintering of the scales has on the oxidation process; the unusual Arrhenius plots at this pressure, revealed in Part I of this work,[8] become straightforward to interpret in terms of this mechanism. It was found that, at 700–900 °C and 0.13 kPa, the initial linear stage ($Q = 40$–$55\,\mathrm{kJ\,mol^{-1}}$) does not significantly differ from those at lower temperatures, 500–600 °C and oxygen pressures, 0.65–13 kPa. However, the subsequent stages at this pressure are realised by a noticeably different mechanism, characterised by negative values of Q, which increase (in absolute value) from 85–90 to 95–110 kJ mol^{-1} for the following parabolic and linear kinetics stages respectively, while m fluctuates between 1/2 and 1/3. So it is quite possible to conclude that the scale, which was nucleated and formed during the first linear stage, sinters and subsequently recrystallises with an apparent enlargement of the contribution from lattice diffusion during the propagation of the oxidation process in the material. These peculiarities shift the process to a gas diffusion regime, which is governed by the permeability of the scale; hence this regime is dependent on the processes relative to recrystallisation (grain growth, evolution of porosity) of oxide–carbon or oxide compositions. However, these processes, in turn, are determined by solid-state diffusion, as was mentioned in Section 3.2.3. Due to the greater segregation of oxide nuclei in the volume of carbide/oxycarbide, and especially in carbide–carbon compositions, the contribution of the sintering of oxide scale to the carbide oxidation process is more significant, and observed at lower temperatures than was found, by Kofstad et al.,[47] during the oxidation of pure titanium metal.

Negative values of Q were found in all stages of the linear–paralinear model throughout this region, at oxygen pressures of 0.65–13 kPa. In the initial linear stage, Q is 20–85 kJ mol^{-1}; afterwards, in the parabolic stage, Q increases to 85–220 kJ mol^{-1} and then slightly decreases in the final linear stage. These values are in good agreement with those gained for the activation energy of the densification process for TiO_2 during the first stage of sintering, corresponding to the plastic flow kinetics mechanism.[48] It is also quite significant that the highest absolute values for Q are in excellent agreement with those for the oxygen lattice diffusion coefficient, calculated from TGA data for the oxidation of metal titanium.[49] At 700–900 °C and 0.65–13 kPa, $m = 1/2$ for the first two stages, being independent of oxidation parameters, so it is suggesting that the defect structure of sintering oxide does not significantly change. The different behaviour of the scale before and after the ridge temperature reflects the intrinsic change in the solid oxidation products. The presence of carbon within the scale during the oxidation of transition metal carbides very often leads to the formation and stabilisation of oxides typically unstable in this range of temperatures.[24,45,50] A similar situation was revealed in this study, as the anatase phase, contained in the oxide scale, was observed up to 800 °C, although, according to XRD analysis data in the recent paper by Zhang et al.,[51] polymorphic transition of the anatase to rutile phases begins at 500 °C and reaches about 95% at 700 °C. Another key observation is that the anatase phase, in contact with carbon, is more chemically stable; this is confirmed by noting that the carbothermic reduction of anatase starts at higher temperatures when compared with those for the rutile phase.[52]

From the obtained experimental data, a convincing argument would be that, during the oxidation of TiC–C HMC, the anatase–rutile phase transition is directly connected with the ridge temperature, as the intensive polymorphic transformation is concurrent with deeper carbon burn-off in the scale (compare Figs. 1 and 8) of the oxidised material. Presumably, the preferential formation of anatase at lower temperatures, as the result of the phase transformation (oxycarbide decomposition) $TiC_{1-x-y-a}O_z \rightarrow TiO_{2-b}C_b$, is connected with a deficiency of energy (exposed temperature) and reagents (oxygen pressure) as the body-centred tetragonal structure of anatase originates from the simpler, face-centred cubic, NaCl structure,[53] which is inherent to the carbide/oxycarbide phase. Hence this structural correspondence simplifies the nucleation process of the novel oxide phase in the initial oxycarbide. The lower density of the anatase (9% less than that of rutile) provides more opportunities for the dissolution of carbon (as well as for diffusion of oxygen) than are available to the rutile structure. During the polymorphic transition, the scale provides much lower protection from oxidation than normal, as the diffusion resistance of the structure is reduced. Throughout the oxidation of TiC–C HMC, the effect of ridge temperature, when the oxidation rate of materials rises rapidly to a maximum and then declines with subsequent growth of temperature, is caused by the accumulated impact of interconnected processes occurring in the scale, such as the accelerated release of carbon oxides and the polymorphic transition, from low- to high-density phases, of titanium oxides. The eventual rise of oxidation temperature leads to a steady decrease of carbon content coupled with a steady increase of rutile fraction in the scale. These factors bring about a significant change in both gas and solid diffusion processes, due to the development of recrystallisation in the oxide and a con-

sequent reduction in gas permeability through the scale. This mechanism is reflected in the kinetics analysis, as at the ridge temperature the sign of the activation energy changes and further increases in oxidation temperature correspond to a decrease of the oxidation rate, although the absolute value of Q does not change significantly as it describes similar solid-state diffusion processes, but with the opposite effect on oxidation rate of the material.

Although no explanation or analysis of the phenomenon was reported before, analogous behaviour has also been observed previously with single-phase carbide materials. For example, Voitovich and Pugach[24] revealed something similar to the effect of ridge temperature at 800 °C for quasi-stoichiometric hot-pressed TiC, which was oxidised in air; the anatase phase was also identified in the oxide scale of samples at higher oxidation temperatures up to 900 °C.

For additional consideration of the ridge parameter phenomenon with respect to the chemical activity of carbon, the reader is referred to Gozzi et al.,[39] who studied many different types of carbon, and also found out the inflection points in the Arrhenius plots for the oxidation kinetics of these materials at a temperature range of about 650–700 °C as, at higher temperatures, the process of oxidation of carbon materials is shifted to the regime where gas diffusion is dominant.

3.2.5. Higher temperatures/higher oxygen pressures

The increase of oxygen pressure at 700–900 °C up to 13–65 kPa brings about a change in the oxidation mechanism of the material. At oxygen pressures higher than the ridge pressure in this temperature range, the values for m are not affected, while the activation energy varies dramatically in both sign and magnitude. The initial stage is characterised by a negligibly small value of Q, whereas afterwards the value fluctuates: 15–30 kJ mol^{-1} for the first parabolic stage, 10–20 kJ mol^{-1} – for the second parabolic and 5–10 kJ mol^{-1} – for the final, second linear stage. All this allows us to classify the current mechanism as a process governed by the different steps of gas interdiffusion through the micro- and nanoporous scale with structure that varies with the evolution of the oxidation process. These rate-determining steps of the oxidation process can include oxygen adsorption, the diffusion of oxygen to the apparent carbide–oxide interface and/or counter diffusion of gaseous products back through the porous medium. The individual identification of these steps is problematic, because some of them are functioning periodically as serial or concurrent processes.

A noticeable characteristic of the oxidation process at the highest studied temperature of 1000 °C is the value of exponent m, which is independent of oxygen pressure and reaches a maximum value for all kinetics stages of $m = 1$, except the final linear stage where m reaches the value of 1/2; probably due to the higher rate of scale recrystallisation inherent to samples oxidised at this temperature.

4. Conclusions

This work has been a physico-chemical study of the phase transformations and transitions during the oxidation of 93 vol% TiC–7 vol% C (graphite) HMC at temperatures of 500–1000 °C and oxygen pressures of 0.13–65 kPa mainly for interpretation of the ridge effect, which was revealed first due to the kinetics phenomenological model developed in the preceding part. The following conclusions concerning this mechanism of the process and oxidation behaviour of TiC–C HMC with low carbon content in general can be drawn:

(1) At lower temperatures/lower oxygen pressures, the initial (linear) oxidation stage is connected with the dissolution of oxygen in the carbide (formation of oxycarbide $TiC_{1-x-y}O_y$) and the subsequent decomposition of the oxycarbide due to oversaturation by oxygen followed later still by the formation of oxide nuclei: $TiC_{1-x-y}O_y \rightarrow TiO_{2-b}C_b + dC(CO, CO_2)$. During the next parabolic stage, the process appears to shift to the solid-state diffusion regime, with oxygen grain boundary diffusion through the anatase $TiO_{2-b}C_b$ as the rate-determining process. The gasification of precipitated carbon in the transition regime between the chemical reaction and gas diffusion stages of carbon oxidation dominates the final (linear) stage of the phenomenological model.
(2) At lower temperatures/higher oxygen pressures, the dominant process during the first stage follows the transition regime between solid-state and gas diffusion oxidation mechanisms. This mechanism is defined by the processes of sintering and grain growth (recrystallisation) development in the scale; being limited by gas diffusion, the rate of oxidation is directly related to the characteristics of porosity within the scale, which in turn are dependent on diffusion parameters in the oxide scale. Throughout the oxidation process in this range of oxidation parameters, this mechanism changes little and remains in the same transition regime, but with a shift to a greater contribution from the gas diffusion mechanism, which dominates the oxidation process completely during the final stage. The ridge oxygen pressure corresponds to the value of oxygen pressure sufficient to reach the stoichiometry of oxidation, when the C/Ti ratio involved in the oxidation reactions, over the entire cycle, matches that of the initial composition of the material. At this ridge pressure, the oxidation (burn-off) of carbon in scale is "catching up" with the oxidation of the metal component, so the final stage is dominated by the interdiffusion of oxygen and carbon oxides gas flows through the porous scale.
(3) At the higher temperatures/lower oxygen pressures, negative values of activation energy were found for all stages, with the exception of the initial stage at the lowest value of pressure. In this range, gas diffusion dominates the oxidation process, which is dependent on the sintering and grain growth, as recrystallisation determines the gas permeability of the scale. Due to the greater segregation of oxide nuclei in the volume of carbide/oxycarbide, especially in carbide–carbon compositions, the contribution of the sintering of scale to the oxidation process is more significant, and observed at lower temperatures than for the oxidation of Ti. Presumably, the structural correspondence of anatase

simplifies the nucleation process of this oxide phase in the oxycarbide. The lower density of the anatase provides more opportunities for the dissolution of carbon as well as for diffusion of oxygen than are available to the rutile structure. The anatase–rutile phase transition is directly connected with the ridge temperature, as the intensive transformation occurs concurrently with the deep carbon burn-off in the oxide scale.

(4) At higher temperatures/higher oxygen pressures, the dominant mechanisms appear to be the different stages of gas interdiffusion through the scale with structure that varies with the evolution of the oxidation process. These rate-determining stages of the oxidation process can include oxygen adsorption, the diffusion of oxygen to the apparent carbide–oxide interface and gaseous products outside through the porous scale.

(5) Aside from providing a much better understanding of the oxidation of refractory transition-metal carbides and carbide–carbon HMC, the results of this work present a potential manufacturing method and can be used for the preparation of oxide protective coatings on the surface of structures made of carbides and related composite materials for high-temperature applications in severe environments like chemically active gaseous flows. Therefore, the next necessary step should be connected with developing and employing the novel quantitative methods of microstructure characterisation for oxide–carbon and oxide scales on HMC.

Acknowledgements

The authors wish to thank Prof. A.R. Beketov, Ural State Technical University, Russia and Prof. G.M. Romantsev, Russian State Professional and Pedagogical University for providing the necessary technological and research facilities. The authors would also like to express their gratitude to Prof. D.K. Ross for support and help in the preparation this work for publishing.

References

1. Hasselman, D. P. H., Becher, P. F. and Mazdiyasni, K. S., Analysis of the resistance of high-*E*, low-*E* brittle composites to failure by thermal shock. *Z. Werkstofftech.*, 1980, **11**(3), 82–92.
2. Mazdiyasni, K. S. and Ruh, R., High/low modulus Si_3N_4–BN composite for improved electrical and thermal shock behaviour. *J. Am. Ceram. Soc.*, 1981, **64**(7), 415–419.
3. Shabalin, I. L., Beketov, A. R., Vlasov, V. G. and Rozhkov, A. S., Oxidation of the titanium carbide–carbon composites at 500–1000 °C. In *Refractory Compounds*, ed. P. S. Kyslyi. Ukrainian SSR Academy of Science Institute for Problems of Materials Science, Kiev, 1981, pp. 129–132.
4. Gorinskii, S. G., Beketov, A. R., Podkovyrkin, M. I., Shabalin, I. L. and Kokorin, A. F., Electrical resistivity of hot-pressed TiC–SiC–C composite materials. *Sov. Powder Metall. Met. Ceram.*, 1982, **21**(11), 867–871.
5. Grushevskii, Ya. L., Frolov, V. F., Shabalin, I. L. and Cheboryukov, A. V., Mechanical behaviour of the ceramics containing boron nitride. *Sov. Powder Metall. Met. Ceram.*, 1991, **30**(4), 338–341.
6. Zhukov, Yu. N., Cherepanov, A. V., Beketov, A. R. and Shabalin, I. L., Inspection of the nonuniformity of a ceramic compact for machining by hardness measurement. *Sov. Powder Metall. Met. Ceram.*, 1991, **30**(4), 349–351.
7. Shabalin, I. L., Tomkinson, D. M. and Shabalin, L. I., High-temperature hot-pressing of titanium carbide–graphite hetero-modulus ceramics. *J. Eur. Ceram. Soc.*, 2007, **27**(5), 2171–2181.
8. Shabalin, I. L., Roach, D. L. and Shabalin, L. I., Oxidation of titanium carbide–graphite hetero-modulus ceramics with low carbon content. I. Phenomenological modeling of the ridge effect. *J. Eur. Ceram. Soc.*, 2008, **28**(16), 3165–3176.
9. McNally, R. N. and Bardhan, P., Oxidation resistance of fused TiC–C compositions containing chromium. *J. Mater. Sci.*, 1983, **18**(4), 1213–1223.
10. Afonin, Yu. D., Shalaginov, V. N. and Beketov, A. R., High-temperature oxidation of carbide–carbon materials of the NbC–C and NbC–TiC–C systems. *J. Appl. Chem. USSR*, 1981, **54**(4), 625–628.
11. Shimada, S. and Kozeki, M., Oxidation of TiC at low temperatures. *J. Mater. Sci.*, 1992, **27**(7), 1869–1875.
12. Shimada, S., A thermoanalytical study of oxidation of TiC by simultaneous TGA–DTA–MS analysis. *J. Mater. Sci.*, 1996, **31**(3), 673–677.
13. Shimada, S., Yunazar, F. and Otani, S., Oxidation of hafnium carbide and titanium carbide single crystals with the formation of carbon at high temperatures and low oxygen pressures. *J. Am. Ceram. Soc.*, 2000, **83**(4), 721–728.
14. Shimada, S. and Mochidsuki, K., The oxidation of TiC in dry oxygen, wet oxygen, and water vapor. *J. Mater. Sci.*, 2004, **39**(2), 581–586.
15. Shimada, S., Onuma, T., Kiyono, H. and Desmaison, M., Oxidation of HIPed TiC ceramics in dry O_2, wet O_2, and H_2O atmospheres. *J. Am. Ceram. Soc.*, 2006, **89**(4), 1218–1225.
16. Gozzi, D., Montozzi, M. and Cignini, P. L., Oxidation kinetics of refractory carbides at low oxygen partial pressures. *Solid State Ionics*, 1999, **123**(1), 11–18.
17. Bellucci, A., Gozzi, D., Kimura, T., Noda, T. and Otani, S., Auger electron spectroscopy analysis of cross-section surface of oxidized titanium carbide single crystal. *J. Am. Ceram. Soc.*, 2003, **83**(12), 2116–2121.
18. Webb, W. W., Norton, J. T. and Wagner, C., Oxidation studies in metal–carbon systems. *J. Electrochem. Soc.*, 1956, **103**(2), 112–117.
19. Münster, A., Über die oxidation metallischer hartstoffe. *Z. Electrochem.*, 1959, **63**(7), 807–818.
20. Macdonald, N. F. and Ransley, C. E., The oxidation of hot-pressed titanium carbide and titanium boride in the temperature range 300–1000 °C. *Powder Metall.*, 1959, **3**, 172–176.
21. Stewart, R. W. and Cutler, I. V., Effect of temperature and oxygen partial pressure on the oxidation of titanium carbide. *J. Am. Ceram. Soc.*, 1967, **50**(4), 176–180.
22. Reichle, M. and Nickl, J. J., Untersuchungen über die Hochtemperaturoxidation von Titankarbid. *J. Less-Common Met.*, 1972, **27**, 213–236.
23. Lavrenko, V. A., Glebov, L. A., Pomitkin, A. P., Chuprina, V. G. and Protsenko, T. G., High-temperature oxidation of titanium carbide in oxygen. *Oxid. Met.*, 1975, **9**(2), 171–179.
24. Voitovich, R. F. and Pugach, E. A., High-temperature oxidation of titanium carbide. *Sov. Powder Metall. Met. Ceram.*, 1972, **11**(2), 132–136.
25. Voitovich, V. B. and Lavrenko, V. A., Oxidation of titanium carbide of different purity. *Sov. Powder Metall. Met. Ceram.*, 1991, **30**(11), 927–932.
26. Schuhmacher, M. and Eveno, P., Oxygen diffusion in titanium carbide. *Solid State Ionics*, 1984, **12**, 263–270.
27. Pavlov, I. E., Zainulin, Yu. G., Alyamovsky, S. I. and Shveikin, G. P., Solubility of hydrogen in cubic titanium oxycarbides. *Sov. Powder Metall. Met. Ceram.*, 1975, **14**(12), 1004–1006.
28. Ivanov, N. A., Andreeva, L. P. and Geld, P. V., Thermal conductivities, electrical resistivities and thermal expansion of titanium carbonitrides and oxycarbides. *Sov. Powder Metall. Met. Ceram.*, 1978, **17**(8), 613–616.
29. Zainulin, Y. G., Alyamovsky, S. I. and Shveikin, G. P., Concerning the structural mechanism of oxygen inclusion into the lattice of titanium carbide. *J. Phys. Chem. Solids*, 1978, **39**(1), 29–31.
30. Afir, A., Achour, M. and Pialoux, A., Etude de la reduction carbothermique du dioxyde de titane par diffraction X a haute temperature sous pression controlee. *J. Alloys Compd.*, 1994, **210**(1–2), 201–208.
31. Afir, A., Achour, M. and Saoula, N., X-ray diffraction study of Ti–O–C system at high temperature and in a continuous vacuum. *J. Alloys Compd.*, 1999, **288**(1–2), 124–140.

32. Kofstad, P., Thermogravimetric studies of the defect structure of rutile (TiO_2). *J. Phys. Chem. Solids*, 1962, **23**, 1579–1586.
33. Haul, R. and Dümgen, G., Sauerstoff-selbstdiffusion in rutilkristallen. *J. Phys. Chem. Solids*, 1965, **26**, 1–10.
34. Irie, H., Watanabe, Y. and Hashimoto, K., Carbon-doped anatase TiO_2 powders as a visible-light sensitive photocatalyst. *Chem. Lett.*, 2003, **32**(8), 772–773.
35. Shen, M., Wu, Z., Huang, H., Du, Y., Zou, Z. and Yang, P., Carbon-doped anatase TiO_2 obtained from TiC for photocatalysis under visible light irradiation. *Mater. Lett.*, 2006, **60**(5), 693–697.
36. Kofstad, P., *High Temperature Corrosion*. Elsevier Applied Science, London/New York, 1988, pp. 206–222, 292–295.
37. Markali, J., An electron microscopic contribution to the oxidation of titanium at intermediate temperatures. In *Proceedings of the 5th International Congress on Electron Microscopy*, ed. S. S. Reese Jr. Academic Press, New York, 1962, pp. C4–C6.
38. Rothschild, A., Komem, Y. and Cosandey, F., The impact of grain boundary diffusion on the low temperature reoxidation mechanism in nanocrystalline $TiO_{2-\delta}$ films. *Interf. Sci.*, 2001, **9**(3–4), 157–162.
39. Gozzi, D., Guzzardi, G. and Salleo, A., High temperature reactivity of different forms of carbon at low oxygen fugacity. *Solid State Ionics*, 1996, **83**(3–4), 177–189.
40. Cascarini de Torre, L. E., Llanos, J. L. and Bottani, E. J., Graphite oxidation in air at different temperatures. *Carbon*, 1991, **29**(7), 1051–1052.
41. Luo, X., Robin, J.-C. and Yu, S., Effect of temperature on graphite oxidation behavior. *Nucl. Eng. Des.*, 2004, **227**(3), 273–280.
42. Thomas, J. M., Microscopic study of graphite oxidation. In *Chemistry and Physics of Carbon*, *vol. 1*, ed. P. L. Walker Jr. Marcel Dekker, New York, 1965, pp. 135–168.
43. Filipuzzi, L. and Naslain, R., Oxidation mechanisms and kinetics of 1D-SiC/C/SiC composite materials. II. Modeling. *J. Am. Ceram. Soc.*, 1994, **77**(2), 467–480.
44. Barrer, R. M., Surface and volume flow in porous media. In *The Solid–Gas Interface*, *vol. 2*, ed. E. Alison Flood. Marcel Dekker, New York, 1967, pp. 557–609.
45. Kuptsov, S. G., Vlasov, V. G., Beketov, A. R., Shabalin, I. L., Fedorenko, O. V. and Pykhteev, Yu. P., Low-temperature oxidation mechanism of zirconium carbide. In *Kinetics and Mechanism of Reactions in Solid State*, ed. E. A. Prodan. Byelorussian State University, Minsk, 1975, pp. 182–183.
46. Afonin, Yu. D., Shalaginov, V. N. and Beketov, A. R., High-temperature oxidation of niobium monocarbide. *J. Appl. Chem. USSR*, 1985, **58**(3 Pt. 1), 423–427.
47. Kofstad, P., Anderson, P. B. and Krudtaa, O. J., Oxidation of titanium in the temperature range 800–1200 °C. *J. Less-Common Met.*, 1961, **3**(2), 89–97.
48. Perez-Maqueda, L. A., Criado, J. M. and Real, C., Kinetics of the initial stage of sintering from shrinkage data: simultaneous determination of activation energy and kinetic model from a single nonisothermal experiment. *J. Am. Ceram. Soc.*, 2002, **85**(4), 763–768.
49. Kofstad, P., Anderson, P. B. and Krudtaa, O. J., High-temperature oxidation of titanium. *J. Less-Common Met.*, 1967, **12**(6), 449–464.
50. Zhilyaev, V. A., Zainulin, Yu. G., Alyamovskii, S. I. and Shveikin, G. P., High-temperature oxidation of zirconium and hafnium oxycarbides and oxycarbonitrides. *Sov. Powder Metall. Met. Ceram.*, 1972, **11**(8), 632–636.
51. Zhang, J., Li, M., Feng, Z., Chen, J. and Li, C., UV Raman spectroscopic study on TiO_2. I. Phase transformation at the surface and in the bulk. *J. Phys. Chem. B*, 2006, **110**(2), 927–935.
52. Setoudeh, N., Saidi, A. and Welham, N. J., Carbothermic reduction of anatase and rutile. *J. Alloys Compd.*, 2005, **390**(1–2), 138–143.
53. Cangiani, G., Ab-initio study of the properties of TiO_2 rutile and anatase polytypes. These N 2667 Pour L'Obtention du Grade de Docteur es Sciences, Ecole Polytechnique Federale de Lausanne, Lausanne, 2003.